

GT2011-46429

## INTEGRATION OF UNKNOWN INPUT OBSERVERS AND CLASSIFICATION FOR TURBOFAN ENGINE DIAGNOSIS

Daoliang Tan\*, Ai He, Xiangxing Kong, Xi Wang

Laboratory of Jet Informatics  
Department of Aerospace Propulsion, Beihang University  
Beijing, China, 100191

### ABSTRACT

A great deal of attention has been attracted in the analytical model-based engine diagnostics over the past years. Meanwhile, an increasing number of researchers and practitioners make an attempt to gain an intelligent diagnoser in a pattern recognition way. A question naturally emerges of how to combine the two techniques to improve the robustness of an on-board diagnostic system. In this context, this paper suggests an integrated approach that combines the unknown input observer (UIO) with the support vector machine (SVM) technique to aircraft engine fault diagnosis. Sensor faults and actuator faults are separately considered. To reduce the effect of engine disturbances on diagnostic performance, we first design a bank of UIOs, each of which is sensitive to all sensor and actuator faults but only one signal. Then, the magnitudes of a set of residuals between the UIO-based estimations and the engine measurements are fed into an SVM classifier to detect and isolate engine faults. Experimental results demonstrate an encouraging potential of the suggested method and that the UIO-oriented approach is superior or competitive to the Kalman-based algorithm.

### NOMENCLATURE

$A_8$	Nozzle area
KF	Kalman filter
LQR	Linear quadratic regulator
MOP	Multiple operating points
$M_f$	Fuel flow

$N_h$	High-pressure turbine speed
$N_h^*$	Maximum $N_h$
$N_l$	Low-pressure turbine speed
$P_3$	High-pressure compressor exit pressure
$P_6$	Low-pressure turbine exit pressure
$T_6$	Low-pressure turbine exit temperature
RBF	Radial basis function
$\mathcal{R}^n$	An $n$ -dimensional real-valued vector space
SOP	Single operating point
SVM	Support vector machine
UIO	Unknown input observer

### 1 Introduction

So far, a large number of efforts have been made to achieve robust model-based diagnostics [1–3]. For example, the UIO theory has attracted many interests from researchers in the fault diagnosis field. The purpose of the UIO is to improve the estimation robustness against model uncertainty (e.g., modeling error and noise). The UIO strengthens the robustness of state estimation by incorporating an explicit term of system disturbances into the state model and nullifying the effect of the disturbances by means of algebraic constraints.

Patton et al. [4] computed the parameters of a UIO estimator based on canonical form transformation, in order to attenuate the impact of model uncertainties (e.g. errors and noise). Later, Chen and Patton [5] simplified the procedure of parameter computation of a full-order UIO, bypassing the canonical transform.

\*Address all correspondence to this author (e-mail:dltan@buaa.edu.cn).

Moreover, Krzemiński and Kaczorek [6] investigated the issue of reduced-order UIO design in an optimization manner. But there is little work that compares the UIO and other estimators—e.g., Kalman filter (KF)—in the diagnostic circumstance.

On the other hand, more and more researchers attempt to handle the issue of fault diagnosis in a pattern recognition way. For instance, Park et al. [7] fused principal component analysis and linear discriminant analysis to extract fault features, whereas Zhou [8] solely used principal component analysis to improve the discriminative power of fault signatures. The learning-based diagnosis, however, does not make full use of a priori knowledge on the dynamical system. A natural question comes into our mind: how can we combine the model-based diagnosis with the classification technique to enhance the diagnostic robustness?

The motivation of this paper is to integrate the model-based UIO technique and the SVM learning for turbofan engine diagnosis. Specifically, we build on an integrated approach that synthesizes a group of UIOs and SVM classifiers for the detection and isolation of aircraft engine faults. A bank of UIOs are designed to nullify the effect of system disturbances on estimation accuracy. Each UIO has a good sensitivity to all sensor and actuator faults but only one signal. The magnitudes of a set of residuals between the UIO-based estimations and the engine measurements are chosen to represent fault characteristics. These signatures are identified by an SVM classifier to detect and isolate engine faults.

This paper is organized as follows. First of all, Section 2 briefly revisits the UIO estimation. Then, Section 3 discusses the generation of engine residual signatures and Section 4 tackles the detection and isolation of engine faults. Moreover, Section 5 gives experimental results based on the simulations of some turbofan engine. Finally, this paper is concluded in Section 6.

## 2 State Estimation with Disturbance

The model-based diagnosis generally requires a mathematical model for the concerned plant. In this paper, we use a linear state-space model to express the operation of an engine. Suppose that the aerodynamics of the engine can be locally described as

$$\dot{x}(t) = Ax(t) + B_{11}w(t) + B_{12}u(t) \quad (1)$$

$$y(t) = Cx(t) + D_{11}w(t) + D_{12}u(t) \quad (2)$$

where  $x(t) \in \mathcal{R}^n$  indicates engine states,  $w(t) \in \mathcal{R}^d$  system disturbances,  $u(t) \in \mathcal{R}^p$  control inputs,  $y(t) \in \mathcal{R}^q$  engine measurements, and  $A$ ,  $B_{11}$ ,  $B_{12}$ ,  $C$ ,  $D_{11}$ , and  $D_{12}$  are consistent matrices.

Assume without loss of generality that  $B_{11}$  is of a full-column rank,  $D_{11} = 0$ , and  $D_{12} = 0$ . This is because we can eliminate the disturbance term  $w(t)$  in the measurement equation (2) using a linear transformation (see Chapter 3 in Ref. [5]) and subtract the component of  $D_{12}u$ —since the control law is

known to us in advance. Therefore, the engine model can be transformed into a commonly desired form.

We demand that an observer of the engine state  $x(t)$  should resist the disturbances  $w(t)$  and have the following form:

$$\dot{z}(t) = Fz(t) + Gu(t) + Hy(t) \quad (3)$$

$$\hat{x}(t) = z(t) + My(t) \quad (4)$$

where  $z(t)$  is observer states and  $\hat{x}(t)$  is the state estimation of  $x(t)$ . In practice, we need to evaluate the unknown observer parameters of  $F$ ,  $G$ ,  $H$ , and  $M$ . An expectation is that the estimation error  $e(t) = x(t) - \hat{x}(t)$  should be as close to zero as possible when  $t \rightarrow \infty$ . A minor manipulation of  $e(t)$  will yield [5]

$$\begin{aligned} \dot{e}(t) = & (A - MCA - H_1C)e(t) - [F - (A - MCA - H_1C)]z(t) - \\ & [H_2 - (A - MCA - H_1C)M]y(t) - [G - (I - MC)B_{12}]u(t) - \\ & (MC - I)B_{11}w(t) \end{aligned} \quad (5)$$

where  $H = H_1 + H_2$ . The purpose of splitting  $H$  into  $H_1$  and  $H_2$  is to facilitate the evaluation of the possible effects of different items on the error dynamics, from the point of view of the mathematical operation. Naturally, we have

$$F - A + MCA + H_1C = 0 \quad (6)$$

$$H_2 - AM + MCAM + H_1CM = 0 \quad (7)$$

$$G - B_{12} + MCB_{12} = 0 \quad (8)$$

$$MCB_{11} - B_{11} = 0, \quad (9)$$

so as to make the observation error  $e(t)$  insensitive to the observer states  $z(t)$ , the engine measurements  $y(t)$ , the control inputs  $u(t)$ , and the system disturbances  $w(t)$ . Then the dynamics of the error  $e(t)$  becomes  $\dot{e}(t) = Fe(t)$ . If all the eigenvalues of the matrix  $F$  lie in the left complex plane, then  $\hat{x}(t)$  must asymptotically approach  $x(t)$ . Based on basic matrix properties, the following results can be easily obtained.

**Theorem 1.** *There exists a matrix  $M$  which satisfies Eqn. (9) if and only if  $\text{rank}(CB_{11}) = \text{rank}(B_{11})$ .*

**Corollary 1.**  *$M = B_{11}[(CB_{11})^T(CB_{11})]^{-1}(CB_{11})^T$  is a special solution to Eqn. (9).*

One physical explanation of the rank constraint in Theorem 1 is that the number of system disturbances should be less than that of available sensor measurements. Further, we can reach the solutions to Eqns. (6)–(8):  $G = B_{12} - MCB_{12}$ ,  $F = A - MCA - H_1C$ , and  $H = H_1 + FM$ , where  $H_1$  is the dual matrix that assigns the poles of the pair  $(A - MCA, C)$  to the expected locations. Figure 1 shows the procedure to compute the

(S<sub>0</sub>) Examine the relation  $\text{rank}(CB_{11}) = \text{rank}(B_{11})$ : If true, go to S<sub>1</sub>; otherwise, go to S<sub>2</sub>.

(S<sub>1</sub>) Compute  $M, G, F,$  and  $H$  by

$$\begin{aligned} M &= B_{11}[(CB_{11})^T(CB_{11})]^{-1}(CB_{11})^T \\ G &= B_{12} - MCB_{12} \\ F &= A - MCA - H_1C \\ H &= H_1 + FM, \end{aligned}$$

where  $H_1$  assigns the expected poles of the pair  $(A^T - A^T C^T M^T, C^T)$ .

(S<sub>2</sub>) There does not exist a UIO and stop.

**FIGURE 1.** Computational procedure for the UIO parameters

UIO parameters. More computational details can also be referred in [5, 6]. It should be noted that this paper just makes use of the full-order observer to estimate the operating state and does not take into account any order reduction of the observer.

### 3 Residual Generation

In reality, it is often difficult to know the real state of a dynamical system, and the available clues reside only in system measurements. Hence diagnostic researchers make full use of system inputs and outputs to diagnose the system. In this paper, we are mainly interested in sensor and actuator faults. The two classes of faults (sensor and actuator) are addressed separately. In general, the deviation  $r(t) = y(t) - \hat{y}(t)$  of the estimated outputs  $\hat{y}(t)$  from the measurements  $y(t)$  is utilized to assist in fault diagnostics. In addition to the previous state monitoring, the diagnosis process consists of fault detection and fault isolation.

#### 3.1 Detection Case

For the task of fault detection, if there occurs a fault in the engine system, then this fault will trigger noticeable variation in the value of  $r(t)$  due to the large mismatch between the predicted engine outputs and the realistic jet measurements; otherwise, the signal  $r(t)$  should remain zero, provided that the estimation of engine states is accurate. In actuality, both control inputs and measured outputs of the engine are used to estimate the engine state  $x(t)$  based on the UIO (Eqns. (3)–(4)), and the subtraction of the estimated output  $\hat{y}(t)$  using Eqn. (2) from the true measurement  $y(t)$  will yield the fault-indicating residual  $r(t)$ . It is worth noting that there does not exist any big difference for the detection of sensor and actuator faults from the point of view of the logic procedure, despite their separate detectors.

### 3.2 Isolation Case

For the isolation of engine faults, the generation of  $r(t)$  will differ for the sensor scenario and the actuator scenario however. This difference originates from the construction of a dynamical model that is essential to the computation of UIO filter parameters. In the sensor scenario, the measurement from the faulty sensor will not arise in the output equation of the dynamical model. On the other hand, the model state will take into account the fault bias in the actuator scenario. In the following, we will give these details.

**3.2.1 Sensor Fault** With regard to the isolation of a fault in one of the engine sensors, this paper creates a group of  $q$  (the number of engine measurements) state estimators, each of which is insensitive to the fault in one specific sensor. The feed into each estimator consists of all the control inputs  $u(t)$  to the engine and the entire engine measurements except the one to whose fault this estimator is immune. Therefore, one different UIO will be given after every application of the procedure listed in Fig. 1 and produces a  $(q - 1)$ -dimensional residual. A total of  $q$  residual vectors can thus be obtained.

As an example, when we are faced with the design of an estimator  $\mathbf{UIO}^i$  that is not affected by the  $i$ -th sensor ( $i = 1, \dots, q$ ), the inputs of the  $\mathbf{UIO}^i$  are composed of engine actuation  $u(t)$  and engine outputs  $y^i(t)$  derived from eliminating the  $i$ -th component  $y_i(t)$ —the measurement of the  $i$ -th sensor—from engine measurements  $y(t)$ . Clearly, the model  $[A, B_{11}, B_{12}, C^i]$  can be used to evaluate the  $\mathbf{UIO}^i$ 's parameters, where  $C^i$  is  $C$  with the  $i$ -th row removed. A residual vector  $r^i(t)$  is thus generated. In a similar way, we can acquire other diagnostic residuals.

For the benchmark Kalman filtering algorithm, the procedure for computing a family of residual vectors will be akin to that used in the UIO case. Additionally, according to the process of generating  $r^i(t)$  ( $i = 1, \dots, q$ ), it is easy to see that  $r^i(t)$  is not related to the measurement of the  $i$ -th sensor which, however, affects other residual vectors  $r^j(t)$  ( $j \neq i$ ). This fact is applicable to both the UIO estimator and the Kalman filter.

**3.2.2 Actuator Fault** By contrast, there exists a slight difference in constructing the dynamical model to produce residual vectors for the actuator fault isolation. Practically, there need to devise  $p$  UIOs ( $p$  is the number of actuation exerted on the engine) for isolating the possible bias fault in one of the actuators. As far as the  $k$ -th UIO ( $k = 1, \dots, p$ ) is concerned, an augmented model is first build on the basis of the original engine description:

$$\dot{\tilde{x}}^k(t) = \tilde{A}^k \tilde{x}^k(t) + \tilde{B}_{11}^k \tilde{w}^k(t) + \tilde{B}_{12}^k u(t) \quad (10)$$

$$y(t) = \tilde{C}^k \tilde{x}^k(t) + \tilde{D}_{11}^k \tilde{w}^k(t) + \tilde{D}_{12}^k u(t) \quad (11)$$

**TABLE 1.** Physical Meaning of Mathematical Symbols

Symbol	Meaning
$f_k$	Faulty bias in the $k$ -th actuator
$\xi_k$	Gaussian white noise
$B_k$	The $k$ -th column of the matrix $B_{12}$
$D_k$	The $k$ -th column of the matrix $D_{12}$

where  $\tilde{x}^k(t) = (x^T \ f_k)^T$ ,  $\tilde{w}^k(t) = (w^T \ \xi_k)^T$ ,  $\tilde{A}^k = \begin{pmatrix} A & B_k \\ 0 & 0 \end{pmatrix}$ ,  $\tilde{B}_{11}^k = \begin{pmatrix} B_{11} & 0 \\ 0 & 1 \end{pmatrix}$ ,  $\tilde{B}_{12}^k = \begin{pmatrix} B \\ 0 \end{pmatrix}$ ,  $\tilde{C}^k = (C \ D_k)$ ,  $\tilde{D}_{11}^k = (D_{11} \ 1)$ , and  $\tilde{D}_{12}^k = D_{12}$ . In the meantime, Table 1 delineates the meanings of  $f_k$ ,  $\xi_k$ ,  $B_k$ , and  $D_k$ . The fault bias  $f_k$ , which might occur in the  $k$ -th actuator, is taken into account by the state vector  $\tilde{x}^k$  of this augmented model to simplify the isolation process.

Hence, the application of the procedure in Fig. 1 to the augmented model (Eqns. (10)–(11)) will produce a **UIO** <sup>$q+k$</sup>  estimator, and a  $q$ -dimensional residual vector  $r^{q+k}(t)$  is further formed. Repeat this process and we can get other **UIO** filters and residual vectors with respect to the remaining actuators. The approach to generate Kalman filter-based residuals is analogous to that used in the UIO context, in terms of the concerned dynamical model.

The method used in this paper differs from the classical UIO diagnosis by Chen and Patton [5] in that rather than viewing the malfunctioned actuation component as a disturbance term, we explicitly consider the bias fault through the state augmentation. In addition, the distinction between the suggested method and the work from Kobayashi and Simon [9] lies in that this paper replaces Kalman filters by the UIOs and makes use of intelligent SVM classifier for fault detection and isolation.

## 4 Engine Fault Detection and Isolation

In the previous section, we discussed the process of producing fault residuals. Unlike earlier diagnostic research that focuses on the aspect of fault residual generation, this paper pays further attention to machine learning-based analysis of residual signatures, since automatic and accurate fault detection and isolation is critical to engine health management.

### 4.1 Detection of Jet Faults

In this paper, the magnitude  $\|r(t)\|$  of the residual vector  $r(t)$  by way of the detection estimator (as described in Subsection 3.1) is extracted to represent the operational characteristics of the engine: fault and health (no fault). The  $\|r(t)\|$  signature is then given to an SVM classifier to know about whether there exists a fault in the engine's sensors and actuators.

The SVM detector is gained as follows: 1) A set of operating data can be collected under the faulty condition and the healthy condition; 2) the data from the faulty mode are labeled as “+1” (positive samples) and those from the healthy mode as “-1” (negative samples); and 3) the labeled data constitute the training samples to the LIBSVM program package [10] to learn an SVM classifier.

Since the performance of the linear kernel is unsatisfactory in detecting engine sensor or actuator faults, the kernel of the SVM classifier is chosen as the radial basis function (RBF). The parameters of the RBF kernel is determined in the grid-searching way, as suggested by the SVM guide [11]. Particularly, this grid includes the penalty parameter  $\mathcal{C}$  and the similarity parameter  $\gamma$ : the value of  $\mathcal{C}$  is discretized in the set  $\{2^{-5}, 2^{-3}, 2^{-1}, 2, 2^3, 2^5, 2^7, 2^9, 2^{11}, 2^{13}, 2^{15}\}$  and the value of  $\gamma$  in the set  $\{2^{-15}, 2^{-13}, 2^{-11}, 2^{-9}, 2^{-7}, 2^{-5}, 2^{-3}, 2^{-1}, 2, 2^3, 2^4\}$ . Finally,  $\mathcal{C} = 0.0315$  and  $\gamma = 0.5$  are selected as the values of the kernel parameters of the SVM detector.

### 4.2 Isolation of Engine Faults

When a fault is detected in the engine system, there needs to find out the source of this fault (which sensor or actuator) to take a prompt action to avoid flight accidents. Similar to fault features in the detection scenario, the magnitude vector  $f = (\|r^1(t)\|, \dots, \|r^q(t)\|)^T$  of this array of residuals  $r^i(t)$  ( $i = 1, \dots, q$ ) serves as sensor fault signatures and the vector  $g = (\|r^{q+1}(t)\|, \dots, \|r^{q+k}(t)\|, \dots, \|r^{q+p}(t)\|)^T$  as actuator fault signatures. All these residuals  $r^j(t)$  ( $j = 1, \dots, q, q+1, \dots, q+p$ ) are obtained by means of the isolation estimators, as is introduced in Subsection 3.2.

Then, the vector of magnitude features is fed into an SVM classifier to figure out where the fault comes from. The SVM isolator is trained in a manner akin to that in the detector circumstance. First, we have to record  $(q+p)$  classes of fault samples and each class corresponds to the failure data in one sensor or actuator. Second, the fault data are labeled consecutively from 1 to  $q+p$ . Once again, the RBF is used to be the kernel of the SVM isolator and the values of the kernel parameters are searched as  $\mathcal{C} = 0.03125$  and  $\gamma = 16$ . Based on this setting, an SVM isolator can be learned using the LIBSVM package.

It should be pointed out that the sensor fault and the actuator fault are independently considered, i.e., two SVM isolators are designed—one for sensor fault classification and the other for actuator fault classification. The use of these paralleled classifiers is because of the inconsistency between sensor fault features and actuator fault ones in the dimension ( $q \neq p$  in general). The Euclidian norm is actually utilized to extract the features required in the fault detection and isolation. In summary, Figure 2 shows the flowchart of the diagnosis procedure used in this paper.

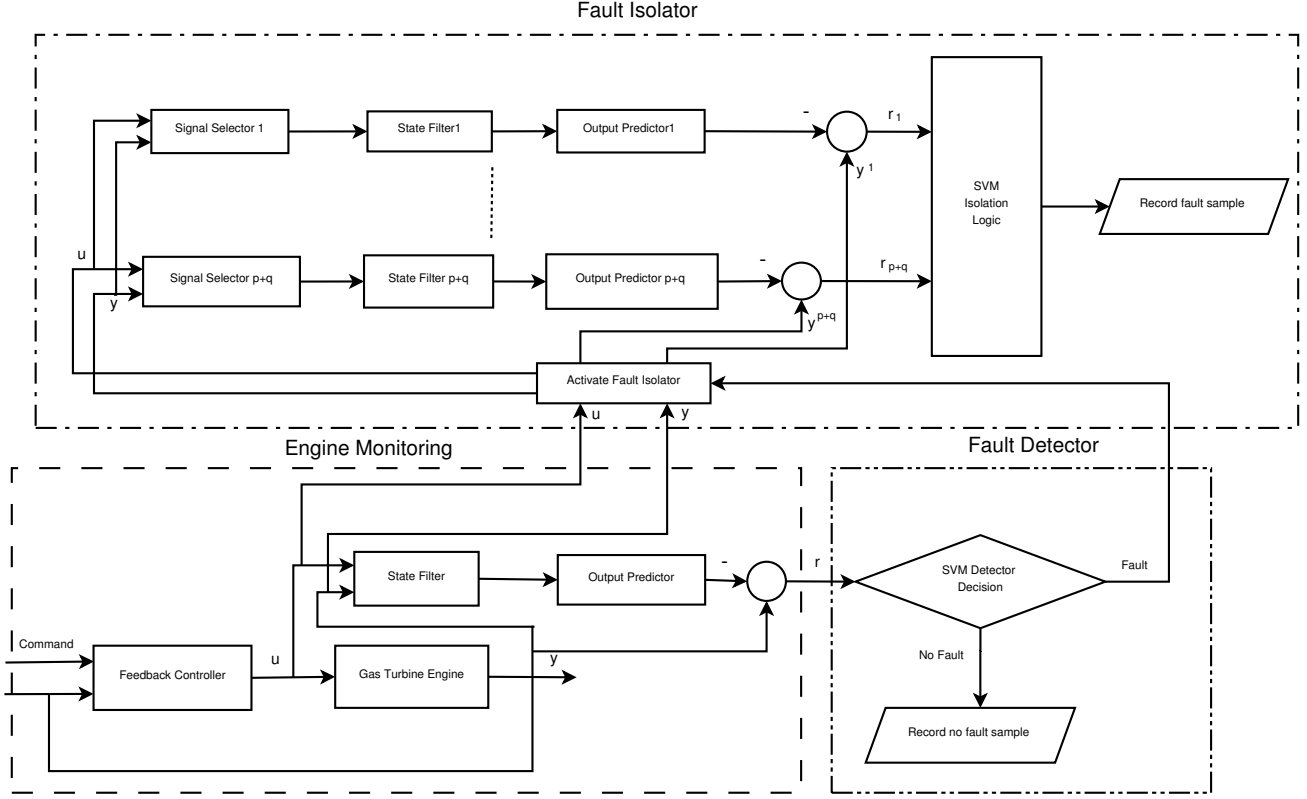


FIGURE 2. Schematic flowchart of the diagnosis procedure

## 5 Experimental Results

In order to validate the performance of the proposed method, we use the high-fidelity model package of one twin-spool turbofan engine to perform simulation experiments. This in-service engine has two control inputs and five measurements: the controlled variables comprise main-burner fuel flow  $M_f$  and nozzle throttle area  $A_8$  and the measured variables include high-pressure rotor speed  $N_h$ , low-pressure rotor speed  $N_l$ , high-pressure compressor exit pressure  $P_3$ , low-pressure turbine exit pressure  $P_6$ , and low-pressure turbine exit temperature  $T_6$ . In addition, this engine is locally controlled by a linear quadratic regulator [12] and we are merely concerned with the operational mode of  $N_h = \text{constant}$  in this paper.

### 5.1 Experiment Design

The fault data are generated using a series of linearized models of this engine at a wide range of operating points from  $67.5\%N_h^*$  to  $100\%N_h^*$ , where  $N_h^*$  is the maximum  $N_h$ . To compare the performance of the UIO-based diagnosis with that of the Kalman-based diagnosis, two kinds of experiments are carried out. One is at a single operating point (SOP) and the other at multiple operating points (MOPs). In the SOP experiments, the training and testing samples both come from the same operating

$$\begin{aligned}
 A &= \begin{pmatrix} -2.2510 & 0.1459 \\ 1.6298 & -1.4982 \end{pmatrix} & B_{11} &= \begin{pmatrix} 0.0500 & 0.2024 \\ 0.0739 & 0.5662 \end{pmatrix} \\
 B_{12} &= \begin{pmatrix} 0.1896 & 0.0419 \\ 0.1550 & 1.7336 \end{pmatrix} & K_{lqr} &= \begin{pmatrix} 18.9874 & 13.7686 \\ -0.5234 & 80.2041 \end{pmatrix} \\
 C &= \begin{pmatrix} 1 & 0 & 1.8592 & 2.4552 & -0.3493 \\ 0 & 1 & 0.3193 & -0.1469 & -0.0506 \end{pmatrix}^T & D_{11} &= \mathbf{0}_{5 \times 2} \\
 D_{12} &= \begin{pmatrix} 0 & 0 & 0.1247 & 0.1374 & 0.2406 \\ 0 & 0 & 0.0134 & -1.5112 & -0.2790 \end{pmatrix}^T
 \end{aligned}$$

FIGURE 3. Engine model parameters at  $85\%N_h^*$

point. Meanwhile, in the MOP experiments, the training data stem from a set of operating points and the testing data from another set of operating points. It should be noted that all the models are normalized and dimensionless.

Specifically, we employ  $85\%N_h^*$  to be the operating point in the SOP experiments. At this operational mode, Figure 3 presents the parameters of the normalized model and its controller. A UIO filter is designed for the  $85\%N_h^*$  model and at the same time is also used to estimate the state of the engine at all the other operating points. The motivation behind one UIO filter is to examine the robustness of the UIO estimator against model

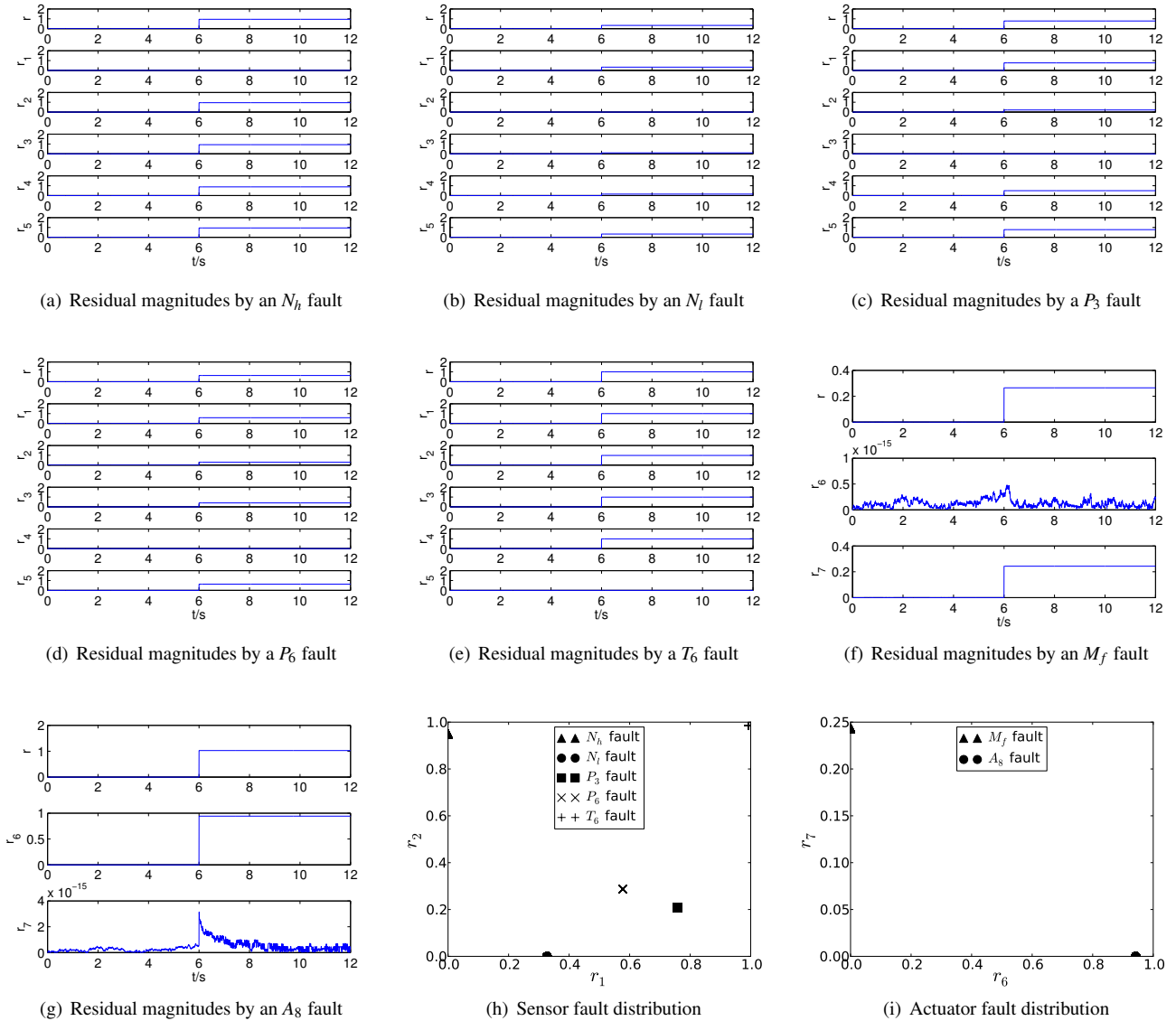


**FIGURE 4.** Residual signatures generated by the UIO method for engine fault detection and isolation in the SOP scenario

variation. For another thing, in the MOP experiments, the set of operating points  $\{67.5\%N_h^*, 75\%N_h^*, 81\%N_h^*, 83\%N_h^*, 85\%N_h^*, 87\%N_h^*, 89\%N_h^*, 91\%N_h^*, 93\%N_h^*, 95\%N_h^*, 97\%N_h^*, 99\%N_h^*\}$  are leveraged to trigger training samples and the set  $\{70\%N_h^*, 77.1\%N_h^*, 82\%N_h^*, 84\%N_h^*, 86\%N_h^*, 88.1\%N_h^*, 90\%N_h^*, 92\%N_h^*, 94\%N_h^*, 96\%N_h^*, 98\%N_h^*, 100\%N_h^*\}$  to induce testing samples.

In the course of simulation experiments, a step fault is automatically activated at the moment of  $t = 6s$  in every fault class. In detail, the sensor faults consist of the measured bias in the  $N_h$ ,  $N_l$ ,  $P_3$ ,  $P_6$ , and  $T_6$  and the actuator faults contain the actuation bias in the  $M_f$  and  $A_8$ . The magnitude of the fault is configured to be one and the white noise with zero mean and unity standard

deviation is added into the engine models to simulate system disturbances. This scheme is also applied to the Kalman method to give a fair comparison. In current study, we do not take into account measurement noise.

## 5.2 Engine Fault Diagnosis in the SOP Scenario

The purpose of the SOP experiments is to illustrate the advantage of the UIO method over the Kalman one from the perspective of fault signatures. Figure 4 depicts UIO-based magnitude signatures in seven abnormalities: five sensor faults— $N_h$ ,  $N_l$ ,  $P_3$ ,  $P_6$ ,  $T_6$ —and two actuator faults— $M_f$ ,  $A_8$ . The detection signature  $\|r(t)\|$  (denoted as  $r$ ) and the isolation signa-

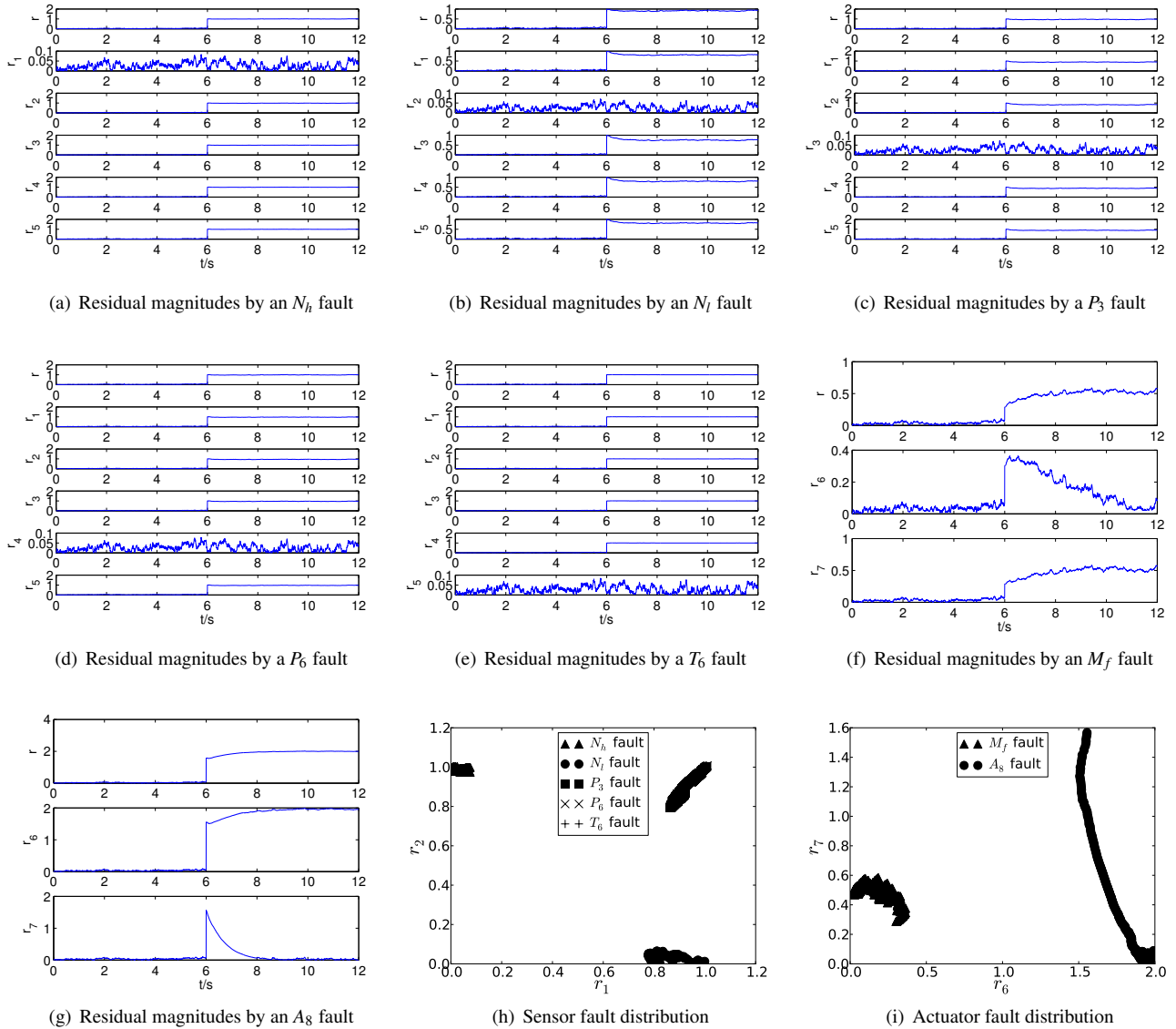


**FIGURE 5.** Residual signatures generated by the KF method for engine fault detection and isolation in the SOP scenario

tures  $\|r^1(t)\| - \|r^5(t)\|$  (denoted as  $r_1 - r_5$ ) for the sensor faults are shown in Subfigs. 4(a)–4(e). Meanwhile, Subfigures 4(f)–4(g) display those signatures for the actuator faults. By plotting the first two features in the two-dimensional plane, Subfigures 4(h)–4(i) visualize the distributions of the sensor and actuator fault signatures (or summarize fault samples in Subfigs. 4(a)–4(g)) in the isolation condition, respectively.

Before  $t = 6s$ , the magnitudes of residuals almost retain zero due to accurate state estimation. When one fault occurs at  $t = 6s$ , all the residual signatures except the one that is insensitive to this fault exhibit an increase from the zero owing to the impact of an incorrect measurement or actuation signal on the estimation.

These facts can be easily seen in Fig. 4.

For instance, if the  $N_h$  sensor malfunctions at  $t = 6s$ , then the detection signature  $r$  (or  $\|r(t)\|$ ) has a sudden rise, compared with its zero value before  $6s$ . In the meantime, each of the isolation signatures  $r_2 - r_5$  gives a differing jump, while the signature  $r_1$  keeps approximately unchanged, for the value of  $r_1$  is immune to the  $N_h$  fault. This can be readily understood from Subfig. 4(a).

The analysis for other fault cases is similar. From the statistical standpoint, the compactness of signature samples in the same fault class and the salient difference between the samples of distinct fault classes shown in Subfigs. 4(h)–4(i) manifest the ease of fault isolation in the UIO-based SOP experiments.

**TABLE 2.** Detection Decision Matrix of Sensor Faults by UIO Signatures in the MOP Experiments

		Predicted State		
		Fault	No Fault	
True State	Fault	39600	0	TPR = 100%
	No Fault	0	41900	FPR = 0%

**TABLE 3.** Detection Decision Matrix of Actuator Faults by UIO Signatures in the MOP Experiments

		Predicted State		
		Fault	No Fault	
True State	Fault	15840	0	TPR = 100%
	No Fault	0	16760	FPR = 0%

Figure 5 delineates the corresponding results for the Kalman method. Analogously, we can decipher Fig. 5 in a way like that used for Fig. 4. Making a comparison between Fig. 4 and Fig. 5 leads us to that the UIO method is superior to the Kalman one in the intra-class compactness and the inter-class disparity. A good pair of intra-class compactness and inter-class disparity are expected to greatly simplify the classification of residual signatures. Actually, we do not present the diagnosis performance in the SOP experiments, as it is trivial to classify these highly clustered residual signatures shown in Figs. 4–5. Instead, the emphasis is laid on the diagnostic accuracy of the MOP experiments.

### 5.3 Engine Fault Diagnosis in the MOP Scenario

Likewise, Figures 6–7 display residual signatures under the MOP condition. These features are generated in the following way. The estimators designed for the  $85\%N_h^*$  setpoint model are used to monitor the state of the engine models extended from  $67.5\%N_h^*$  to  $100\%N_h^*$  as well. At each operating point, a bunch of fault signatures can be extracted according to the simulation setting in Subsection 5.1. As a consequence, the features on the twelve training operating points (see Subsection 5.1) are collectively plotted in Figs. 6–7. Figures 6–7 demonstrate that the UIO signatures outperform the Kalman ones not only from the point of view of temporal steadiness but also from the perspective of cluster compactness. The assessment of the diagnostic performance, however, are highly desirable for quantitative metrics.

The metrics recommended by Simon et al. [13] are adopted in this paper to evaluate the accuracy of the UIO- and KF-based

**TABLE 4.** Detection Decision Matrix of Sensor Faults by KF Signatures in the MOP Experiments

		Predicted State		
		Fault	No Fault	
True State	Fault	39420	180	TPR = 99.5%
	No Fault	566	41334	FPR = 1.4%

**TABLE 5.** Detection Decision Matrix of Actuator Faults by KF Signatures in the MOP Experiments

		Predicted State		
		Fault	No Fault	
True State	Fault	15810	30	TPR = 99.8%
	No Fault	1378	15382	FPR = 8.2%

approaches. In practice, the detection decision matrix and the Kappa coefficient are used for the detection evaluation and the classification confusion matrix and the Kappa coefficient are for the isolation evaluation. The Kappa coefficient is a metric that sums up general diagnosis performance to facilitate algorithm assessment. On one hand, the detection decision matrix can be further deduced to calculate True Positive Rate (TPR) and False Positive Rate (FPR) that are defined as the percentage of correctly detected faults in the population of failure samples and the proportion of wrongly detected faults with respect to the total nonfaults, respectively. On the other hand, the classification confusion matrix can be utilized to provide Percent Correctly Classified (PCC) [13] for the various fault classes. For each fault type, PCC is represented as the ratio of the number of correct recognitions of samples belonging to the fault of interest to the entire number of examinations in this fault class. As an extension of PCC, we also describe diagnostic performance using detection/classification accuracy which is computed as the fraction of correctly classified data in the whole samples.

**5.3.1 Fault Detection Evaluation** Tables 2–3 give the detection decision matrices and related TPRs and FPRs for the sensor and actuator faults using the UIO-based signatures. The performance metrics due to the KF-induced features are shown in Tables 4–5. We can see from these tables that the UIO method achieves perfect detection performance (as is listed in Tables 2–3), whereas the Kalman approach might raise false alarms or miss reasonable notifications (as is indicated in Tables 4–5).

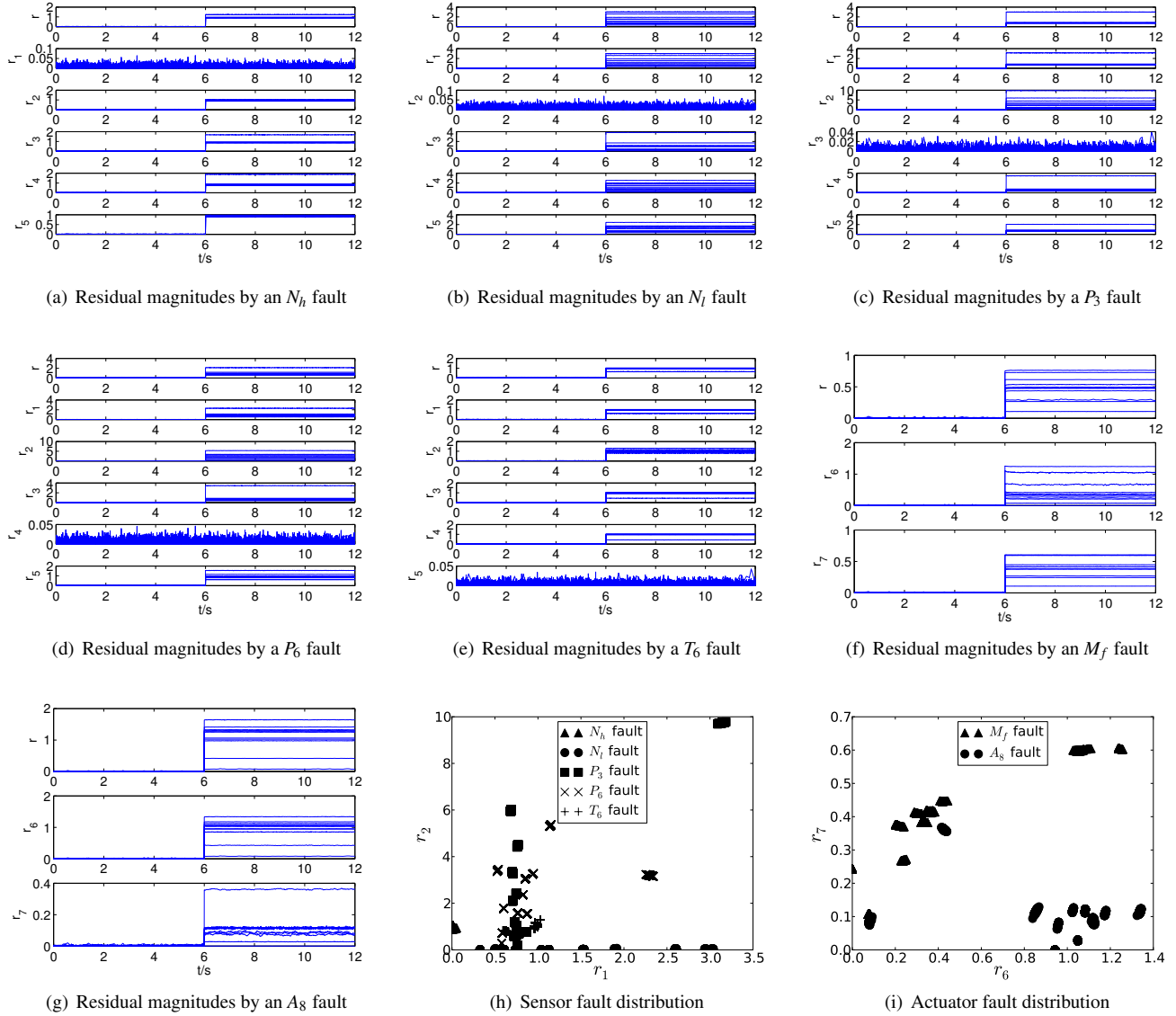


**FIGURE 6.** Residual signatures generated by the UIO method for engine fault detection and isolation in the MOP scenario

**TABLE 6.** The Kappa Coefficient and Detection Accuracy for the Sensor and Actuator Faults in the MOP Experiments

	UIO+SVM		KF+SVM	
	Sensor Fault	Actuator Fault	Sensor Fault	Actuator Fault
Kappa Coefficient	100%	100%	98.168%	91.375%
Detection Accuracy	100%	100%	99.085%	95.681%

The disparity in the number of nonfaults in between Table 2 and Table 3 comes from that the numbers of sensors and actuators are different. Moreover, Table 6 shows the Kappa coefficient and overall accuracy metrics for the sensor and actuator fault mon-

itoring. It can be noted from Table 6 that the UIO signature is better than the Kalman one in engine fault detection, in terms of the Kappa coefficient and detection accuracy. In brevity, the UIO algorithm can bring more desirable detection performance.

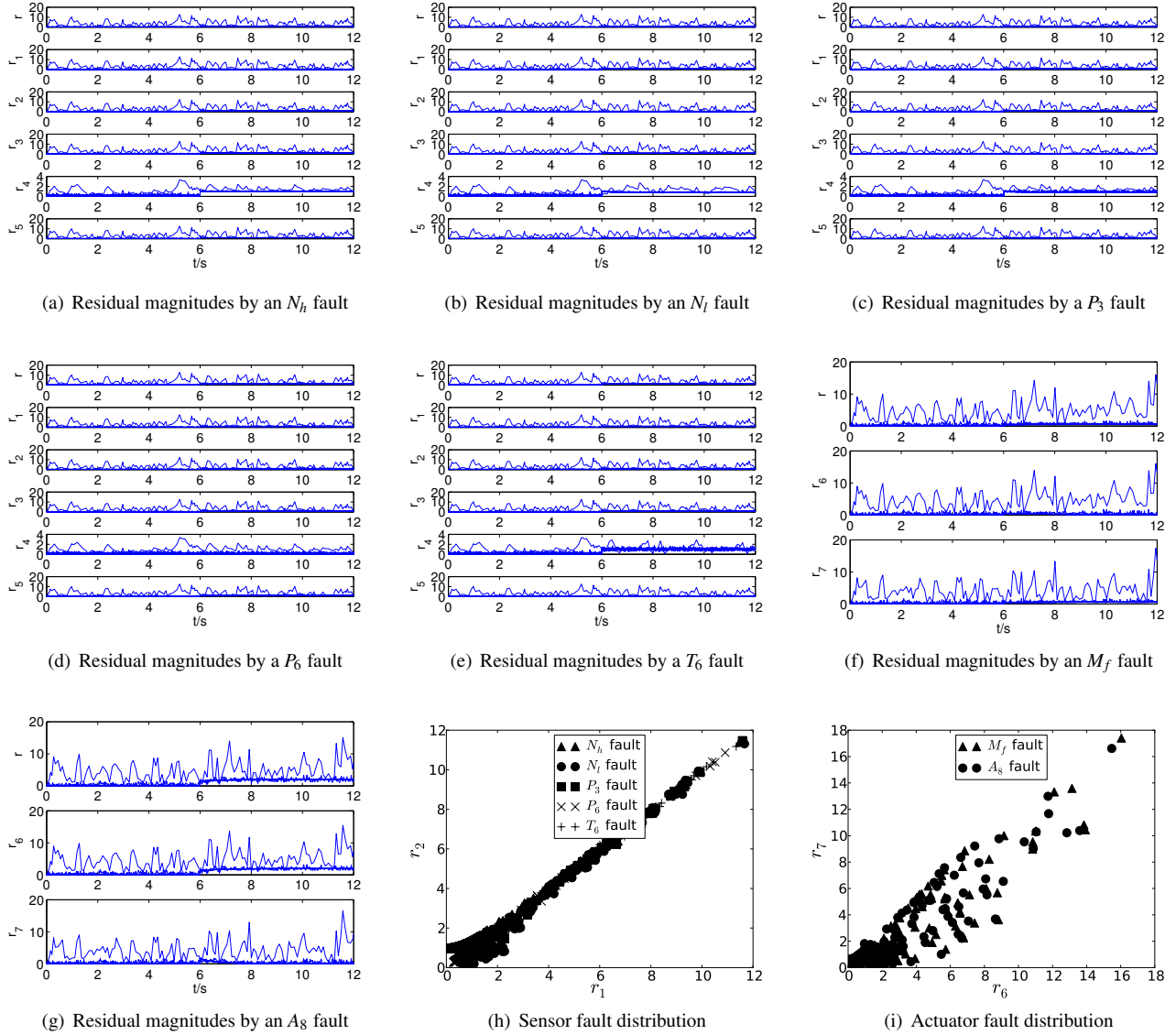


**FIGURE 7.** Residual signatures generated by the KF method for engine fault detection and isolation in the MOP scenario

**5.3.2 Fault Isolation Evaluation** Table 7 presents the classification confusion matrix and its inferred PCC metric for the combination of the UIO signatures with the SVM classifier. It can be safely claimed that the UIO and SVM combination almost produce satisfying PCC performance apart from the  $A_8$  fault. By contrast, Table 8 tabulates the corresponding metrics of the Kalman-based method. We can notice that aside from the  $A_8$  fault, the Kalman approach is a bit inferior to the UIO method with reference to the PCC metric.

In addition, Table 9 records the Kappa coefficient and classification accuracy metrics of the UIO and KF approaches in the MOP fault isolation experiments. It seems that for the isolation

of sensor faults the UIO and SVM integration is slightly superior to the fusion of the KF signatures and the SVM classifier. But the UIO approach is weaker than the Kalman one for the experiments of actuator fault isolation, in terms of both the Kappa coefficient and classification accuracy. Nonetheless, the UIO-oriented diagnosis solution is comparable to that provided by the Kalman-based scheme.

Thus far, the current study has considered the sole magnitude of engine faults: unity one (i.e., 100% bias if the maximum is one relative to the normalized model). Hence one natural question involves what about the effect of smaller fault magnitudes on the diagnostic performance. In this situation, this order of

**TABLE 7.** Classification Confusion Matrix and PCC by UIO+SVM in the MOP Experiments

	$N_h$	$N_l$	$P_3$	$P_6$	$T_6$	$M_f$	$A_8$	PCC
$N_h$	7920	0	0	0	0	0	0	100%
$N_l$	0	7876	0	44	0	0	0	99.4%
$P_3$	0	0	7920	0	0	0	0	100%
$P_6$	0	0	0	7920	0	0	0	100%
$T_6$	0	0	0	0	7920	0	0	100%
$M_f$	0	0	0	0	0	7920	0	100%
$A_8$	0	0	0	0	0	1201	6719	84.8%

fault magnitudes 0.0001, 0.001, 0.01, and 0.1 (corresponding to 0.01%, 0.1%, 1%, and 10% bias) were additionally triggered to create synthetic data samples for diagnostic simulation. The experimental setting is like the one for the unity magnitude case. Figure 8 displays the Kappa coefficient and classification accuracy metrics for the MOP isolation of sensor and actuator faults with different fault magnitudes. The performance of the KF approach is worse than that of the UIO one at moderately smaller magnitudes; both the UIO and Kalman diagnosis, however, are unable to give satisfactory results at such tiny 0.01% magnitude. In short, the UIO-based algorithm is competitive to the Kalman one for engine fault diagnosis.

## 5.4 Discussion

The state estimator and the fault classifier differentiate the proposed method and the pioneering work by Dewallef et al. [14]. Instead of the KF in Ref. [14], this paper exploits the UIO technique that can deal with non-white noise to estimate engine state. Furthermore, the SVM classifier is employed in this work to diagnose engine faults, rather than Bayesian Belief Network used in Ref. [14].

This paper makes an implicit assumption that the category of a detected engine fault is known in isolation—it belongs to a sensor failure or an actuator one. This assumption does not greatly weaken the applicability of the suggested method. In fact, using input and output signals selection, we can seamlessly incorporate the scheme of Fault Class Isolation [15] into the proposed method to automatically figure out this category. For the sake of space limitation, this paper does not explore this issue in depth.

Another issue is related to the under-determined challenge when there exist more system disturbances than available measurements. In reality, the UIO method can not be directly used to address the under-determined issue. Fortunately, we can leverage the idea of parameter reduction (e.g. the research work in Refs. [16, 17]) to satisfy the rank constraint in Theorem 1. This

**TABLE 8.** Classification Confusion Matrix and PCC by KF+SVM in the MOP Experiments

	$N_h$	$N_l$	$P_3$	$P_6$	$T_6$	$M_f$	$A_8$	PCC
$N_h$	7849	0	0	71	0	0	0	99.1%
$N_l$	0	7807	0	113	0	0	0	98.6%
$P_3$	0	0	7867	52	1	0	0	99.3%
$P_6$	0	0	0	7915	5	0	0	99.9%
$T_6$	0	0	0	24	7896	0	0	99.7%
$M_f$	0	0	0	0	0	7861	59	99.3%
$A_8$	0	0	0	0	0	7	7913	99.9%

will be left as future work and be beyond the scope of this paper.

Currently, this paper does not consider health parameters in the engine model. One may be skeptical of the effect of engine deterioration on diagnosis performance. It appears that the on-line SVM learning offers a promising remedy as long as we are able to acquire a diversity of training samples beforehand under different deteriorating conditions. Alternatively, we can add an explicit term of health factors that are viewed as unknown disturbances into the engine model and apply the proposed framework once again. The shortcoming of our research work is that we require that there should exist only one fault at a time. The future work will investigate the problem of multiple fault diagnosis for the engine system.

## 6 Conclusions

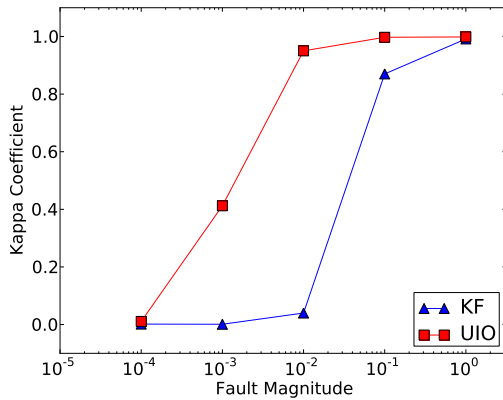
This paper has investigated an approach that combines the UIO estimator with the SVM classifier learning to perform the robust diagnosis of aircraft engine systems. To improve the robustness of engine diagnostic, the effect of system disturbances is nullified by a set of algebraic constraints. A variety of magnitude signatures are extracted to represent distinct fault characteristics and are recognized by an SVM classifier. In terms of the intra-class compactness and the inter-class disparity, the suggested method outperforms the KF-based algorithm in the SOP simulation experiments of one turbofan engine. In the MOP experiments, the UIO signatures are superior or competitive to the KF ones, measured by the conventional diagnostic metrics. All these illustrate an encouraging potential of this proposed approach. Finally, it is worthwhile to explore the multiple faults diagnosis and the under-determined issue in our future work.

## ACKNOWLEDGMENT

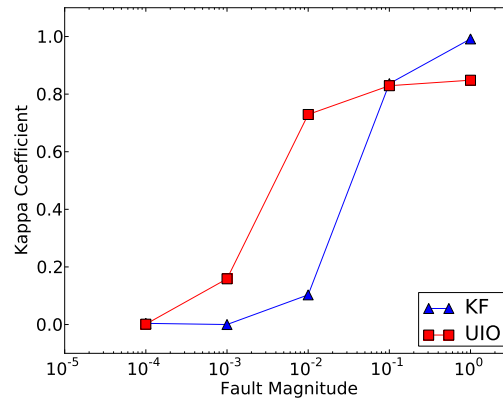
This work is supported by the Aerospace Science Foundation of China (Grant No. 2009ZB51). We thank the anonymous

**TABLE 9.** The Kappa Coefficient and Classification Accuracy for the Sensor and Actuator Faults in the MOP Experiments

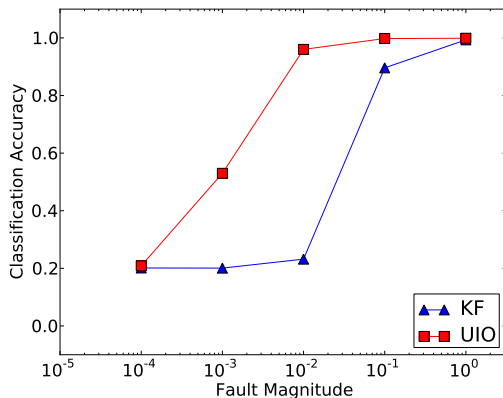
	UIO+SVM		KF+SVM	
	Sensor Fault	Actuator Fault	Sensor Fault	Actuator Fault
Kappa Coefficient	99.861%	84.836%	99.160%	99.167%
Classification Accuracy	99.889%	92.418%	99.328%	99.583%



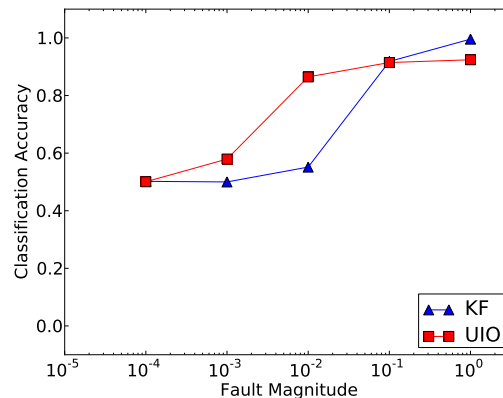
(a) Kappa coefficient in sensor faults



(b) Kappa coefficient in actuator faults



(c) Classification accuracy in sensor faults



(d) Classification accuracy in actuator faults

**FIGURE 8.** MOP isolation performance with respect to different fault magnitudes

reviewers' comments and suggestions for improving the quality of this paper.

## REFERENCES

- [1] Dewallef, P., and Lonard, O., 2003. "On-line performance monitoring and engine diagnostic using robust kalman filtering techniques". In Proceedings of ASME Turbo Expo 2003, no. GT2003-38379.
- [2] Zhang, X., Polycarpou, M., and Parisini, T., 2008. "Design and analysis of a fault isolation scheme for a class of uncer-

tain nonlinear systems". *IFAC Annual Reviews in Control*, 32(1), pp. 107–121.

- [3] Tang, L., Zhang, X., DeCastro, J., Farfan-Ramos, L., and Simon, D., 2010. "A unified nonlinear adaptive approach for detection and isolation of engine faults". In Proceedings of ASME Turbo Expo 2010, no. GT201022642.
- [4] Patton, R. J., Frank, P. M., and Clarke, R. N., eds., 1989. *Fault diagnosis in dynamic systems: theory and application*. Prentice-Hall, Inc., Upper Saddle River, NJ, USA.
- [5] Chen, J., and Patton, R. J., 1999. *Robust model-based fault*

- diagnosis for dynamic systems*. Kluwer Academic Publishers, Norwell, MA, USA.
- [6] Krzemiński, S., and Kaczorek, T., 2004. “Perfect reduced-order unknown-input observer for standard systems”. *Bulletin of the Polish Academy of Sciences Technical Sciences*, **52**(2), pp. 103–107.
  - [7] Park, W., Lee, S., Joo, W., and Song, J., 2007. “A mixed algorithm of pca and lda for fault diagnosis of induction motor”. In *Advanced Intelligent Computing Theories and Applications. With Aspects of Artificial Intelligence*, D.-S. Huang, L. Heutte, and M. Loog, eds., Lecture Notes in Computer Science. Springer Berlin / Heidelberg, pp. 934–942.
  - [8] Zhou, S., Zhang, J., and Wang, S., 2004. “Fault diagnosis in industrial processes using principal component analysis and hidden markov model”. In *Proceedings of American Control Conference 2004*, Vol. 6, pp. 5680–5685.
  - [9] Kobayashi, T., and Simon, D. L., 2003. “Application of a bank of kalman filters for aircraft engine fault diagnostics”. In *Proceedings of ASME Turbo Expo 2003: Power for Land, Sea and Air*, pp. 461–470.
  - [10] Chang, C.-C., and Lin, C.-J., 2001. *LIBSVM: a library for support vector machines*. Software available at URL <http://www.csie.ntu.edu.tw/~cjlin/libsvm>.
  - [11] Hsu, C.-W., Chang, C.-C., and Lin, C.-J., 2010. A practical guide to support vector classification. Tech. rep., Department of Computer Science and Information Engineering, National Taiwan University, Taipei 106, Taiwan.
  - [12] Hofbauer, W., Dolovai, P., Joergl, H., and Hirzinger, J., 2006. “Lqg/ltr controller design for a gas engine”. In *Industrial Electronics, 2006 IEEE International Symposium on*, Vol. 3, pp. 1631–1636.
  - [13] Simon, D. L., Bird, J., Davison, C., Volponi, A., and Iversen, R. E., 2008. “Benchmarking gas path diagnostic methods: a public approach”. In *Proceedings of ASME Turbo Expo 2008*, no. GT2008-51360.
  - [14] Dewallef, P., Romessis, C., Léonard, O., and Mathioudakis, K., 2006. “Combining classification techniques with kalman filters for aircraft engine diagnostics”. *Journal of Engineering for Gas Turbines and Power*, **128**(4), pp. 281–287.
  - [15] Chen, W., and Saif, M., 2008. “Fault class isolation in linear systems with unknown inputs”. In *American Control Conference*, pp. 1600–1605.
  - [16] Simon, D. L., and Garg, S., 2010. “Optimal tuner selection for kalman filter-based aircraft engine performance estimation”. *Journal of Engineering for Gas Turbines and Power*, **132**(3), pp. 031601–1–031601–10.
  - [17] Borguet, S., and Léonard, O., 2010. “A sparse estimation approach to fault isolation”. *Journal of Engineering for Gas Turbines and Power*, **132**(2), pp. 021601–1–021601–7.